



# Effects of quenching rate on amorphous structures of $\text{Cu}_{46}\text{Zr}_{54}$ metallic glass

Jiangting Wang<sup>a,b</sup>, Peter Damian Hodgson<sup>a</sup>, Jingde Zhang<sup>b</sup>, Wenyi Yan<sup>c</sup>, Chunhui Yang<sup>a,d,\*</sup>

<sup>a</sup> Centre for Material and Fibre Innovation, Deakin University, Waurn Ponds, VIC 3217, Australia

<sup>b</sup> Key Lab for Liquid Structure and Heredity of Materials of Ministry of Education, Shandong University, Jinan 250061, China

<sup>c</sup> Department of Mechanical Engineering, Monash University, Clayton, VIC 3800, Australia

<sup>d</sup> School of Engineering and Information Technology, Faculty of Science and Technology, Deakin University, Waurn Ponds, VIC 3217, Australia

## ARTICLE INFO

### Article history:

Accepted 6 October 2008

### Keywords:

$\text{Cu}_{46}\text{Zr}_{54}$  metallic glass  
Molecular dynamics  
Amorphous state  
Quenching rate

## ABSTRACT

Metallic glass shows some superior properties different from crystalline, but the nature of amorphous structure and structural change during glass transition have not been completely understood yet. Molecular dynamics simulation provides intuitive insight into the microstructure and properties at atomistic level. Before probing into the microstructures of metallic glass with molecular dynamics (MD) simulation, it is important to obtain amorphous state first. In the current work, we reproduce the process of manufacturing metallic glass in laboratory including the melting, equilibrating and quenching procedure with molecular dynamics simulations. The structure changing at melting point and glass transition temperature are investigated with the different cooling processing. The partial radial distribution function (PRDF) is applied as a criterion to judge the final amorphous state obtained considering the quenching at different cooling rates and the effects of cooling rate on the formation of amorphous structures are further discussed.

© 2008 Elsevier B.V. All rights reserved.

## 1. Introduction

Metallic glass (MG) is of great interest in both academic and industry because of its excellent mechanical properties and its potential structural applications. In general, MG has much higher yield point and less ductility, which is thought to be a reflection of the difference in the deformation and fracture mechanisms between MG and crystalline alloys (Wang et al., 2004). In the last two decades, metallic glasses have regained considerable interest due to the fact that new glass-forming compositions have a critical cooling rate of less than 100 K/s and the glassy can be made in the dimension of 1 cm or more. The development of such alloys with a very high resistance to crystallization of the undercooled melt needs the enhanced understanding of the fundamentals on both their liquid state and glass transition (Loffler, 2003).

Molecular Dynamics (MD) simulation is a widely used numerical tool in exploring microstructural effects in metals at the atomistic level. MD simulation with millions of atoms can investigate collective phenomena, such as melting, phase transitions and plastic deformation (Mendeleev and Ackland, 2007). For example, it

can reproduce the process of melting and quenching through a glass transition. Therefore, MD models give valuable insight into the topological features of the local structure at melting and upon vitrification (Deng et al., 1989). Recently MD simulations were conducted to investigate local structure, glass formation ability and mechanical properties, etc. (Lee et al., 2003; Falk and Langer, 1998; Li and Li, 2006). As the first step to investigate metallic glass' properties, generating metallic glass sample through rapid cooling is crucial, in this work, we simulate the melting and quenching of  $\text{Cu}_{46}\text{Zr}_{54}$  to form metallic glass with MD method and the effects of cooling rates are studied systematically.

## 2. Molecular dynamics simulation of forming amorphous metal system

### 2.1. Potential functions for MD simulation

The most essential factor in MD simulation is the interatomic potential which governs the movement of atoms. For metals, their delocalized electrons mean that pairwise additive potentials, like Lenard–Jones potential, are inadequate in accounting for many properties, such as the Cauchy discrepancy of the elastic constants, vacancy formation energies, stacking fault energies, surface structure, and relaxation properties (Daw and Baskes, 1984; Finnis and Sinclair, 1984; Cleri and Rosato, 1993). Based on such considerations, various semi-empirical many-body interatomic potentials were developed to reproduce the thermodynamic and structural

\* Corresponding author at: School of Engineering and Information Technology, Faculty of Science and Technology, Deakin University, Waurn Ponds, VIC 3217, Australia. Tel.: +61 3 52272082; fax: +61 3 5227 2167.

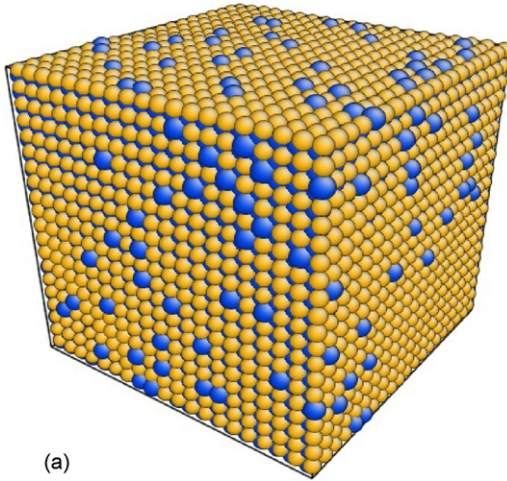
E-mail addresses: [jiangting.wang@deakin.edu.au](mailto:jiangting.wang@deakin.edu.au) (J. Wang), [peter.hodgson@deakin.edu.au](mailto:peter.hodgson@deakin.edu.au) (P.D. Hodgson), [zhangjingde@sdu.edu.cn](mailto:zhangjingde@sdu.edu.cn) (J. Zhang), [wenyi.yan@eng.monash.edu.au](mailto:wenyi.yan@eng.monash.edu.au) (W. Yan), [chunhui.yang@deakin.edu.au](mailto:chunhui.yang@deakin.edu.au) (C. Yang).

properties of metals with good accuracy, such as the Embedded-Atom Model (EAM) developed by Daw and Baskes (1984), the Finnis–Sinclair (FS) model proposed by Finnis and Sinclair (1984) and the Second-Moment Approximation of the Tight-Binding scheme (TB-SMA) developed by Cleri and Rosato (1993). The essential band character of the metallic bond, a many-body treatment over the conceptually and practically simpler pair-potential description is the ability to better reproduce some basic features of metallic systems. The potential adopted in this work is a many-body potential in the TB-SMA scheme. The TB-SMA potential is a relatively simple scheme for relating the atomic and electronic structure, in which the ion–ion interaction is described as made up of an effective band term plus a short-range repulsive pair potential.

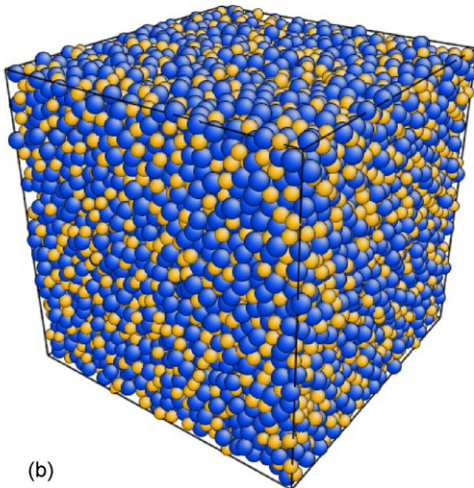
It is well known that the cohesive properties of transition metals and their alloys originate from the large d-band density of states. The band energy can be written for an atom  $i$  as

$$E_B^i = - \left\{ \sum_{i \neq j} c_{\alpha\beta}^2 \exp \left[ -2q_{\alpha\beta} \left( \frac{r_{ij}}{r_0^{\alpha\beta}} - 1 \right) \right] \right\}^{1/2} \quad (1)$$

where  $r_{ij}$  represents the distance between atoms  $i$  and  $j$ , and  $r_0^{\alpha\beta}$  is the first-neighbors distance in the  $\alpha\beta$  lattice.  $c_{\alpha\beta}$  is an effective hopping integral, and  $q$  describes its dependence on the relative interatomic distance. Both  $q$  and  $c_{\alpha\beta}$  are assumed to depend only on the interacting atomic species  $\alpha$  and  $\beta$ .



(a)



(b)

Fig. 1. 3D simulation box of the  $\text{Cu}_{46}\text{Zr}_{54}$  system: (a) starting state at 0 K and (b) final amorphous state.

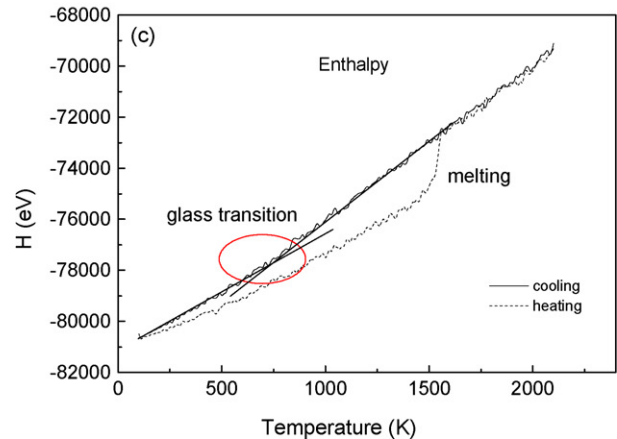
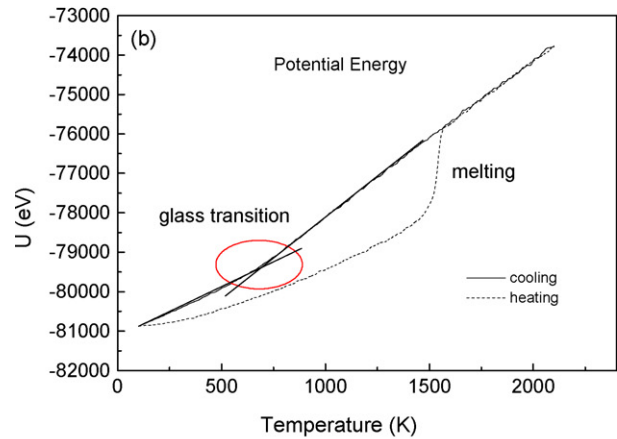
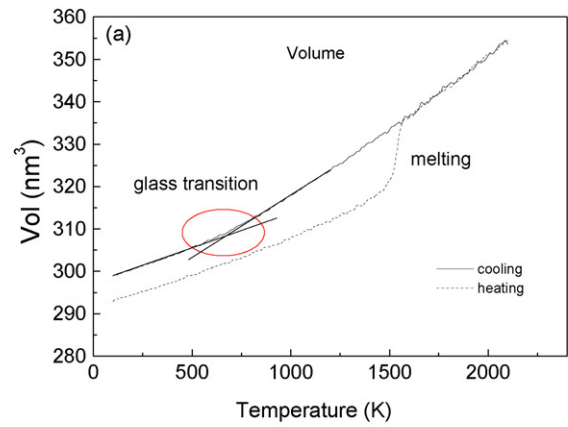


Fig. 2. Volume, potential energy and enthalpy variation as a function of temperature during heating and cooling at rate of 4 K/ps: (a) volume, (b) potential energy and (c) enthalpy.

The repulsive interaction term is assumed to be pairwise and described by a sum of Born–Mayer ion–ion repulsions

$$E_R^i = \sum_{i \neq j} \frac{1}{2} \varepsilon_{\alpha\beta} \exp \left[ -p_{\alpha\beta} \left( \frac{r_{ij}}{r_0^{\alpha\beta}} - 1 \right) \right] \quad (2)$$

The total cohesive energy is

$$U_{tot} = \sum_i (E_B^i + E_R^i) \quad (3)$$

The potential's parameters are fitted to the QM calculated data such as lattice constants, cohesive energies, and bulk module (Duan et al., 2005).

## 2.2. Partial radial distribution function (PRDF)

Usually, liquid and amorphous structure has broad peaks, indicating a degree of disordering. To judge such disordering-amorphous states of metals, the partial radial distribution function is applied. It is a pair correlation function, which describes how the atoms in a system are radially packed on average around each other. This function gives the probability of finding a pair of atoms within a distance  $r$  apart, relative to the probability expected for a completely random distribution at the same density. It is a particularly effective way of describing the average structure of disordered molecular systems such as liquids and amorphous structure. The PRDF can be measured experimentally from X-ray or neutron diffraction studies, thus providing a direct comparison between experimental and simulation. In general, the PRDF,  $g_{\alpha\beta}(r)$ , can be taken in the following form:

$$g_{\alpha\beta}(r) = \frac{V}{N_{\alpha}N_{\beta}} \left\langle \frac{\sum_i n_i^{\alpha\beta}(r)}{4\pi r^2 \Delta r} \right\rangle \quad (4)$$

in which  $n_i^{\alpha\beta}(r)$  is the mean number of  $\alpha\beta$  pair in a shell of width  $\Delta r$  at distance  $r$ ,  $V$  is the volume of the system,  $N_{\alpha}$  and  $N_{\beta}$  are numbers of atom  $\alpha$  and atom  $\beta$ , respectively.

## 2.3. MD modeling of forming amorphous system

In the current study, the MD simulations were performed on a three-dimensional cubic cell with 16,000 atoms using the classical molecular dynamics code LAMMPS (Plimpton, 1995). Periodic boundary condition (PBC) is applied in all three dimensions. The Nose–Hoover barostat (Hoover, 1986), implemented by Melchionna et al. (1993), was used to control the pressure constantly at zero and

to update positions and velocities at each timestep. The integration timestep was chosen to be one fs for all MD simulations.

The system depicted in Fig. 1 was started with arranging Zr and Cu atoms on to a B2 structure lattice, then replacing 4% Cu atoms with Zr atoms randomly. We melted the system by heating the temperature from 0 K to 2100 K in 525 ps, leading to a heating rate of  $4 \times 10^{12}$  K/s. During heating, the particle velocities were rescaled by 1 K increments then equilibrated the system for 250 timesteps at each temperature. The system was found to be melted at 1550 K. Continuing to heat it up to 2100 K was aimed to obtain well-equilibrated liquid state. After heating, the system was equilibrated for 500 ps, which is supposed to be relatively long enough to equilibrate liquid system.

Starting from the well-equilibrated  $\text{Cu}_{46}\text{Zr}_{54}$  liquid, we cooled the system at series of different cooling rates. The cooling method was the same as the heating method above-mentioned. After cooling down to 300 K, the system was kept at constant temperature and constant pressure (NPT) equilibrating for 50 ps. The potential energy, volume, and enthalpy at 300 K were extracted from the equilibrating and averaged over time, which becomes more meaningful than an instant state. The final amorphous states formed with different cooling rates were analyzed to distinguish cooling rates' effects on metallic glass' microstructures and properties.

The simulation setting and atom coordinates of certain state in the melting and quenching were stored for the future use in numerical testing of mechanical properties of metal glass.

## 3. Numerical result and discussion

The whole process of producing  $\text{Cu}_{46}\text{Zr}_{54}$  metallic glass was simulated in the current MD analysis including the melting, equilibrating, and cooling procedures. Fig. 2 shows the volume, potential

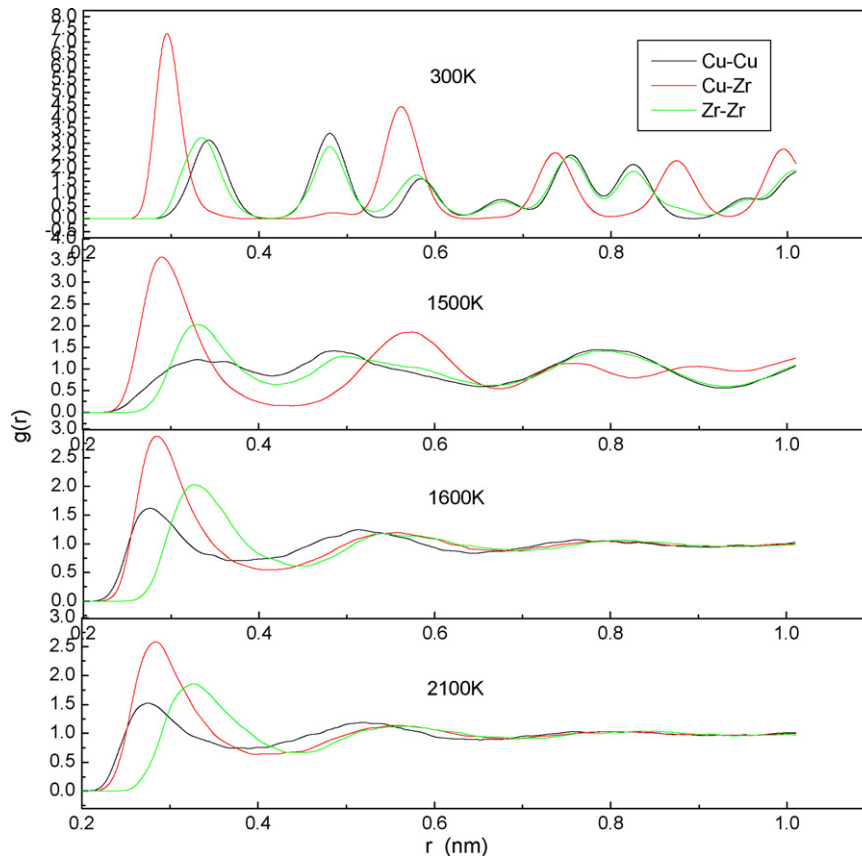


Fig. 3. The PRDFs of the system at temperature 300 K, 1500 K, 1600 K, and 2100 K during heating.

energy, and enthalpy changing as a function of temperature in heating and cooling both at rate of 4 K/ps. During heating, the first-order transition occurs at temperature  $1550 \pm 50$  K, which indicating the melting of B2  $\text{Cu}_{46}\text{Zr}_{54}$  alloy. The large and discontinuous changing in volume, potential energy, and enthalpy reflect the rearrangement in atomic structure, from order to disorder. Above melting point, the cooling curve and heating curve match well. However, the cooling curve shows a change of its slope at temperature  $700 \pm 50$  K, especially obvious in potential energy curve. It means glass transition occurs in this temperature.

At the melting point, a great change in atomic structure happens. Fig. 3 shows the PRDF of the system at different temperatures of 300 K, 1500 K, 1600 K, and 2100 K during heating. At 300 K, it shows a typical B2 structure pattern. The first-nearest neighbors are the unlike atoms peaking at distance of 2.9 Å, while the second-nearest neighbors are the like atoms peaking around 3.4 Å. Before melting, up to 1500 K, the atom types of first-nearest neighbors are not changed, but the peaks are getting less intensive and broader due to the increasing of heat motion. After melting, at 1600 K, the short-range order of atoms changes significantly. The Cu–Cu pair becomes the first-nearest neighbor, following Cu–Zr as the second and Zr–Zr as the third. At a longer distance, the peaks at the range of 0.4–0.6 nm, which are clearly separated at 1500 K, merge together into a low and broad peak at 1600 K. The same phenomenon occurs at the range of 0.7–0.9 nm. A great short-range order change occurred between 1500 K and 1600 K. The PRDF shows no apparent structure order at long distance as peaks merged and getting broader. Above the melting point, the PRDF has non-zero values at all separations and the various previously observed peaks fuse into three broad and spread-out peaks. The changes in the PRDF at melting reflect the changes and smearing out of structural order. Along the increasing amplitudes of atom motions, atoms overcome the structural constraints and then evolve into a liquid state.

After melting, no significant change occurred in short-range order, but the peaks becoming lower. The system was equilibrated at 2100 K for 500 ps, and the liquid states were stored at each 100 ps interval. The analysis of PRDFs at each instant shows little difference between equilibrating time, but the peaks get subtly broader as the equilibrating time increasing. But, keep in mind that the actual equilibrating time includes not only equilibrating at 2100 K, but also the time for heating from melting point to 2100 K, which is around 125 ps.

At the glass transition temperature, the change of volume, potential energy, and enthalpy are very subtle and there is no dramatic drop in these intensive amounts. In the PRDFs, the splitting of the second peak occurs at different temperature for different pairs. Fig. 4 shows the PRDFs of Cu–Cu pair, Cu–Zr pair, and Zr–Zr pair at different temperature during cooling at 4 K/ps. The PRDF of final state at  $T=300$  K retains the overall shape of the liquid phase. The splitting of second peak occurs during cooling from 2100 K to 300 K, at distinct temperature for different atom pairs. This split is indicative of amorphous atomic packing and is observed experimentally in all metallic glass, but not in liquids. The splitting can be explained as the result of peak narrowing (Bailey et al., 2004). As the thermal motion decreases, the peaks are getting narrower. Thus, the splitting of the second peak does not mean any structural transition. At the second-nearest neighbor distance, the structure of liquid state remains as the as those in the cooling-down stage.

Starting from the well-equilibrated liquid state, we cooled the system from 2100 K down to 300 K. A series of different cooling rates, which are listed in Table 1, were adopted to investigate cooling rates' effect on the formation of final metallic glass state. All the cooling rates applied in current simulations lead to the formation of metallic glass. After cooling, a group of metallic glass samples were obtained. The PRDFs of these samples are as shown in Fig. 5. The PRDFs of all these samples are very similar, only exhibit slight

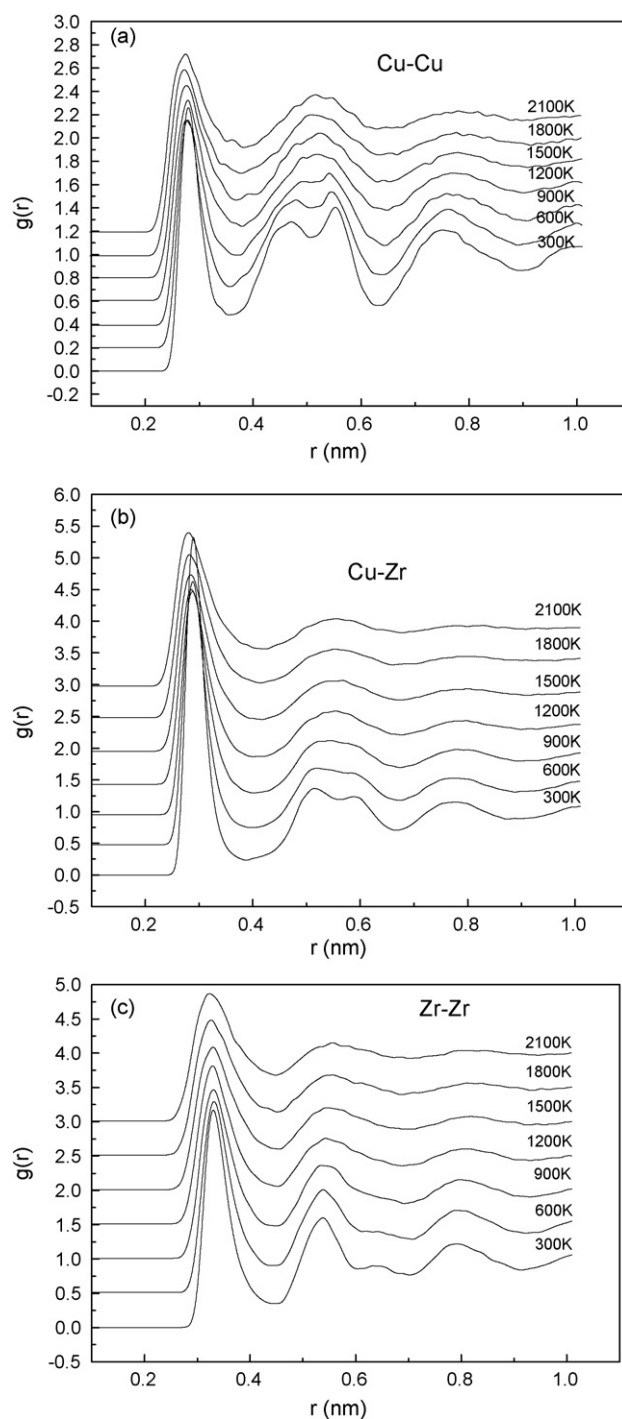
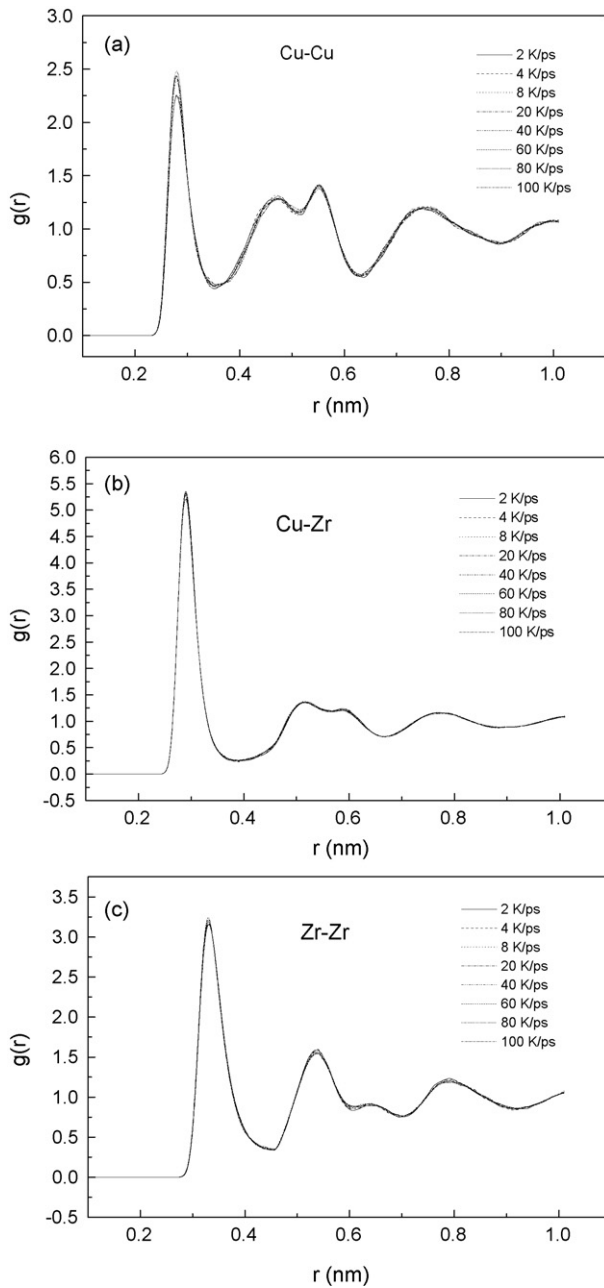


Fig. 4. The PRDFs of Cu–Cu pair, Cu–Zr pair, and Zr–Zr pair at different temperatures during cooling at 4 K/ps: (a) Cu–Cu pair, (b) Cu–Zr pair and (c) Zr–Zr pair.

Table 1  
Different cooling rates adopted during quenching.

Samples	$R_{\text{cooling}}$ (K/ps)
I	2
II	4
III	8
IV	20
V	40
VI	60
VII	80
VIII	100



**Fig. 5.** The PRDFs of final state obtained formed by cooling at series of different cooling rates: (a) Cu–Cu pair, (b) Cu–Zr pair and (c) Zr–Zr pair.

difference in the first peak for Cu–Cu pair, while that of Cu–Zr pair and Zr–Zr pair show a good consistence. The different behaviors shown in Cu–Cu pair, Cu–Zr and Zr–Zr pair suggests that the cooling rate have more effect on the Cu atoms' movement than on Zr. One possible explanation can be the size of atom Zr, 1.58 Å is larger than that of atom Cu, 1.27 Å, so the Cu atoms have higher mobility than Zr atoms. The change of cooling rates have more significant effect on rearrangement of Cu atoms, while do not affect Zr atoms too much. So as the cooling rate decreasing, the degree of disorder for Cu atoms increases more than Zr atoms.

Considering it is a statistical value, PRDF will inevitably miss a great deal of information about the atomic structure. The different cooling rates adopted during quenching are listed in Table 1. The volume, potential energy, and enthalpy are increasing with the increasing cooling rate exponentially. The curves of these three variables as functions of cooling rate,  $R_{cooling}$ , are depicted in Fig. 6.

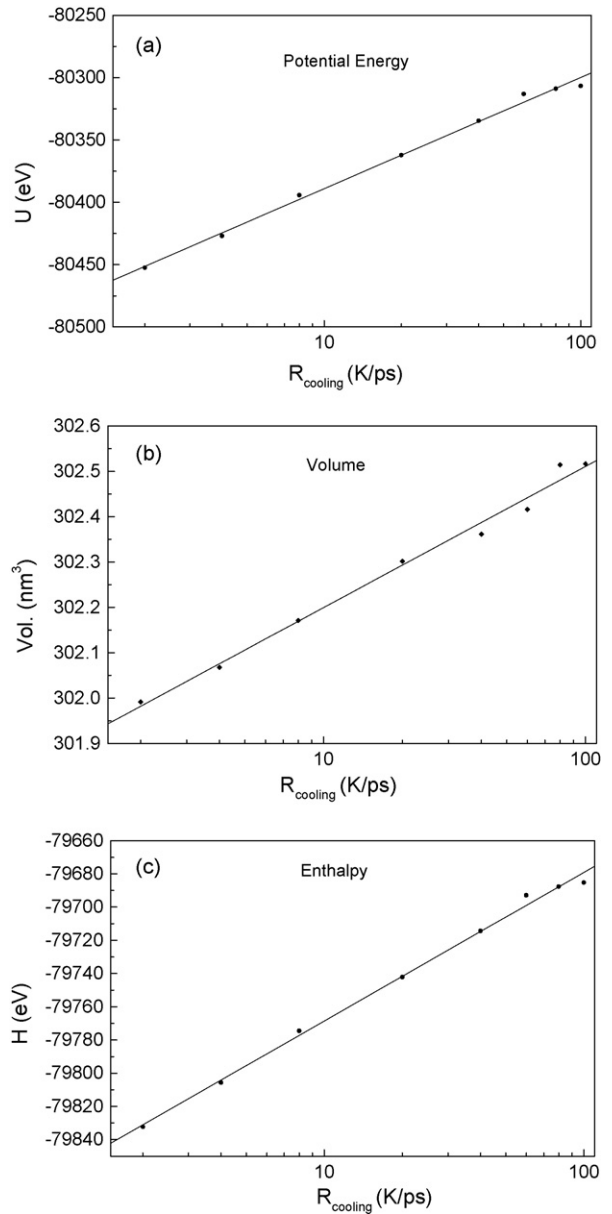


**Fig. 6.** The potential energy, volume and enthalpy of amorphous state change as a function of cooling rate: (a) potential energy, (b) volume and (c) enthalpy.

According to the free-volume theory (Cohen and Grest, 1979), excess free-volume in liquid will be trapped into the glassy state when cooling a liquid into a glass. The quantity of free-volume depends on the cooling rate. The sample cooled at 2 K/ps shows a relatively lower volume and energy, which indicates a more closely packed structure in the final amorphous state. The faster the cooling rate that metallic glass experiences the more excess free-volume exists. From another point of view, slower cooling rate allows more equilibrating time, which in turn gets more free-volume annihilated.

#### 4. Summary

In the current study, the melting, equilibrating and quenching process were simulated to produce amorphous structure of metallic glass using molecular dynamics (MD) method. At melting point, the significant structural change occurs from the rearrangement of short-range order. The amorphous structure in liquid state was

remained during the quenching at rapid cooling rate. Different cooling rates take no apparent effects on the short-range order of final amorphous state in the present MD simulation. However, lower cooling rates lead to denser packing and better equilibrated final state as well as lower volume and potential energy, while higher cooling rates may capture more free-volume for amorphous structures obtained.

### Acknowledgements

The authors would like to appreciate the financial supports from Australian Research Council (ARC) through Prof. Peter Hodgson's Federation Fellowship (FF0455846). The relevant MD simulations were mainly performed using the resources and facilities in APAC and VPAC, Australia with compliments.

### References

- Bailey, N.P., Schiøtz, J., Jacobsen, K.W., 2004. Simulation of Cu–Mg metallic glass: thermodynamics and structure. *Phys. Rev. B* 69, Art. No. 144205.
- Cleri, F., Rosato, V., 1993. Tight-binding potential for transition metals and alloys. *Phys. Rev. B* 48 (1), 22–33.
- Cohen, M.H., Grest, G.S., 1979. Liquid–glass transition, a free-volume approach. *Phys. Rev. B* 20, 1077–1098.
- Daw, M.S., Baskes, M.I., 1984. Embedded-atom method: derivation and application to impurities, surfaces, and other defects in metals. *Phys. Rev. B* 29, 6443–6453.
- Deng, D., Argon, A.S., Yip, S., 1989. Philosophical transactions of the Royal Society of London. Series A. Math. Phys. Sci. 329 (1608), 549–573.
- Duan, G., Xu, D., Zhang, Q., Zhang, G., Cagin, T., Johnson, W.L., Goddard III, W.A., 2005. Molecular dynamics study of the binary  $\text{Cu}_{46}\text{Zr}_{54}$  metallic glass motivated by experiments: glass formation and atomic-level structure. *Phys. Rev. B* 71, Art. No. 224208.
- Falk, M.L., Langer, J.S., 1998. Dynamics of viscoplastic deformation in amorphous solids. *Phys. Rev. E* 57, Art. No. 7192.
- Finnis, M.W., Sinclair, J.F., 1984. A simple empirical N-body potential for transition metals. *Philos. Mag. A* 50, 45–55.
- Hoover, W.G., 1986. Constant-pressure equations of motion. *Phys. Rev. A* 34, 2499–2500.
- Lee, H.-J., Cagin, T., Johnson, W.L., Goddard III, W.A., 2003. Criteria for formation of metallic glasses: the role of atomic size ratio. *J. Chem. Phys.* 119 (18), 9858–9870.
- Li, Q.-K., Li, M., 2006. Atomic scale characterization of shear bands in an amorphous metal. *Appl. Phys. Lett.* 88, Art. No. 241903.
- Loffler, J.F., 2003. Bulk metallic glasses. *Intermetallics* 11, 529–540.
- Melchionna, S., Ciccotti, G., Holian, B.L., 1993. Hoover NPT dynamics for systems varying in shape and size. *Mol. Phys.* 78 (3), 533–544.
- Mendelev, M.I., Ackland, G.J., 2007. Development of an interatomic potential for the simulation of phase transformations in zirconium. *Philos. Mag. Lett.* 87 (5), 349–359.
- Plimpton, S.J., 1995. Fast parallel algorithms for short-range molecular dynamics. *J. Comp. Phys.* 117, 1–19.
- Wang, W.H., Dong, C., Shek, C.H., 2004. Bulk metallic glasses. *Mater. Sci. Eng. R* 44, 45–89.